RMK D Geometric Calibration and its Accuracy Potentials

EuroCOW 2010: The calibration and orientation workshop

February 10-12, 2010, Castelldefels, Spain

Mostafa Madani, PhD

Intergraph Corporation
170 Graphics Drive, Madison, Alabama 35758
Email: Mostafa.Madani@Intergraph.com

KEY WORDS: Digital Aerial Camera, Camera Calibration, Systematic Error Modeling, Accuracy, Aerial Triangulation, Self-calibration Bundle Adjustment

ABSTRACT

Intergraph's RMK D, a true metric medium-format digital camera, was introduced at ISPRS 2008 Congress in Beijing, China. RMK D is particularly designed to replace film-based aerial cameras for smaller photogrammetry projects at very high accuracy. RMK D, with a high frame rate of 1.3 second, captures RGB and NIR images simultaneously and features a compact design with digital forward motion compensation. RMK D includes a customized CCD with an effective size of 6096 x 6846 pixels at 7.2 microns and two Solid State Disk (SSD) storage devices.

An accurate camera calibration method provides reliable values for focal length, principal point coordinates, lens distortion, and other camera systematic errors. Traditionally, cameras are calibrated in laboratories either by using goniometers and collimator banks or by using special test fields of various ranges in sophistication. These techniques enable corrections for the camera distortions to a considerable extent, but leave very small systematic errors due to their own limitations. Correction grids generated by analyzing the image residuals by collocation and self-calibration bundle adjustment are some techniques to model the remaining systematic errors.

This paper overviews the RMK D technical specifications, provides its geometric calibration procedures, and finally gives some preliminary results on its geometrical accuracy. This study revealed that the expected accuracy of less than 0.3 of a GSD (Ground Sample Distance) for planimetry and about 0.6 GSD for vertical can be achieved. More RMK D cameras will be calibrated and flown at different GSDs. An exhaustive geometrical accuracy report will be published later.

1. INTRODUCTION

Photogrammetry has undergone significant change in the last 20 years. The charge-coupled device (CCD), invented about forty years ago, was proven to be an excellent

image sensor. Today, there exist many digital aerial sensors with different resolutions and formats in the market.

Intergraph's Digital Mapping Camera (DMC) was introduced into the market in early 2003. Today, about 100 DMCs are in operation and thousands of the DMC projects have been successfully flown by different customers all over the world. All these DMC projects achieved the required accuracy standards for different photogrammetric applications established by several organizations such as ASPRS, NMAS, etc. (Madani, et. al, 2004).

Intergraph introduced its true medium-format digital camera, called RMK D, at ISPRS 2008 Congress in, Beijing, China. The RMK D includes with two Solid State Disk (SSD) storage devices and carries a small footprint inside the aircraft. This results in low weight and power requirements that allow it to fit in small, single-engine aircraft. As a medium-format camera, the camera is designed to fill the need for small area, engineering, and corridor mapping.

In the following sections, the RMK D specifications and its geometric calibration procedures are given. Some preliminary accuracy results on its geometric accuracy potential are also provided.

2. RMK D TECHNICAL FEATURES

Intergraph's Z/I Imaging RMK D is a medium-format aerial imaging system designed to meet the high-accuracy/high-resolution requirements of engineering mapping and remote sensing tasks. It is ideal for film camera owners seeking to enter the digital acquisition arena and offers a very high geometric accuracy.

RMK D is a true metric multi-spectral sensor with 5760 x 6400 pixels image format and allows you to fly RGB and NIR simultaneously at 1:1 color resolution. Its large field of view results in an excellent Height to Base ratio of 2.4. The combination of 7.2 µm per pixel and the 45mm focal length results in an image scale of about 1:11,000 with a GSD of 8cm at an altitude of 500m. The camera can operate up to an altitude of 8000m non-pressurized and is qualified for the temperature range from -20° - +40°C. The camera is equipped with 2 integrated SSD cartridges to capture 2000 or optionally 4000 images. The weight of 56kg (with 2 SSD cartridges) qualifies RMK D for usage in small aircraft (Doerstel, 2009).

One important requirement for the camera was to support high forward overlaps of up to 80%. To achieve this goal the camera can be operated in two modes selectable during runtime. The high-quality readout mode allows a minimum of 2-second frame rate, whereas a high-speed readout mode will allow down to a1.3-second cycle rate, depending on the solid state disk performance. Internally this is realized by reading the sensor from either one or two corners.

Figure 1. RMK D with 4 MS camera heads, video camera (center) and space for additional sensor

RMK D uses very high-quality optics, CCD, and shutter. Its optics consists of a customized lens system designed and manufactured by Carl Zeiss (Doering, 2009). The CCD is a 42-megapixel DALSA sensor developed exclusively for Intergraph.
The shutter represents the last remaining moving part in the digital camera and consists of 7 blades. To guarantee constant behavior over the lifetime of app. 100,000 cycles, this device is equipped with a unique "non-aging" technique. During open and close cycles the actual position of the blades is measured with a frequency of 100µsec. By using these sample values an internal real-time control algorithm adjusts for any mechanical deviation caused by temperature, pressure or humidity.

One of the main capabilities of RMK D is to deliver images for classification purposes - to supplement remotely-sensed data or to allow delivery into the growing market for image data with absolutely-calibrated radiometry. To achieve this, a new radiometric sphere and new calibration techniques are designed. To preserve the absolute radiometry of the images it is recommended to work with non-destructive Look Up Tables (LUT). The absolute calibration not only improves the visual perception of images by better relative adjustment of the individual camera heads but also enhances radiometric uniformity across multiple cameras (Ryan, 2009).

3. CAMERA GEOMETRIC CALIBRATION

Traditionally, cameras are calibrated in laboratories and their systematic distortions are modeled to a considerable extent, but they always leave some kind of residual systematic errors due to their own limitations.

Different calibration methods are used to model a camera's lens distortion and to compute its interior orientation parameters (Madani, 1985):

- Laboratory Calibration (In-door calibration)
- In-situ System Calibration and Verification (Out-door calibration)

3.1 Laboratory Calibration

In-door or Laboratory calibration is completely separated from actual object photography. Calibration is usually carried out either by using laboratory equipment such as goniometers and collimator banks, or by using special test fields of various ranges in sophistication such as a 3-D cage. The mathematical model used in this method is normally based on the central projection equations, which are extended for interior orientation parameters, radial, and decentring lens distortion.

The in-door camera calibration is expected to provide accurate estimates of the interior orientation parameters which can be used as prior information in the in-situ calibration procedure for a total system calibration.

3.2 In-Situ System Calibration and Verification

In-situ or Test-field calibration is generally in closer conformance to operational circumstances than the laboratory calibration methods. The camera should undergo a total system calibration under operational conditions where the boresight parameters relating the camera and the GPS/INS units are also estimated. This approach requires an array of signalized and highly-accurate control points. The mathematical model for test field calibration is usually similar to that used for laboratory calibration.

3.3 Self-Calibration

Self-calibration is defined as the functional extension of the Collinearity equations.

$$F_x = (x - x_p) + c\frac{U}{W} + \Delta x = 0$$
$$F_y = (y - y_p) + c\frac{V}{W} + \Delta y = 0\,. \qquad (1)$$

Using the auxiliaries

$$\begin{bmatrix} U \\ V \\ W \end{bmatrix} = \mathbf{M} \begin{bmatrix} X - X_C \\ Y - Y_C \\ Z - Z_C \end{bmatrix}$$

where

x, y	image coordinates
c	focal length
x_p, y_p	principal point of auto collimation (PPAC)
X, Y, Z	object coordinates
X_C, Y_C, Z_C	perspective center coordinates
M	an orthogonal rotation matrix that rotates object coordinate axes parallel to corresponding image coordinate

Different two-dimensional additional parameter (AP) models (physical, geometrical, or combinations of both) are used for expressing the unaccounted systematic distortions. Brown (1976) model and variations of it is used very often for calibrating analog and digital cameras in aerial and close-range applications.

Brown model may be expressed as:

$$\Delta x = \Delta x_p - (\bar{x}/c)\Delta c + a_1\bar{x} + a_2\bar{y} + \bar{x}[K_1 r^2 + K_2 r^4 + K_3 r^6] + P_1(r^2 + 2\bar{x}^2) + 2P_2\bar{x}\bar{y} + a_3\bar{x}\bar{y} + a_4\bar{x}^2\bar{y} + a_5\bar{x}\bar{y}^2 + a_6\bar{x}^2\bar{y}^2 + \bar{x}/c[a_{11}(\bar{x}^2 - \bar{y}^2) + a_{12}\bar{x}^2\bar{y}^2 + a_{13}(\bar{x}^4 - \bar{y}^4)]$$

$$\Delta y = \Delta y_p - (\bar{y}/c)\Delta c + \bar{y}[K_1 r^2 + K_2 r^4 + K_3 r^6] + 2P_1\bar{x}\bar{y} + P_2(r^2 + 2\bar{y}^2) + a_7\bar{x}\bar{y} + a_8\bar{x}^2\bar{y} + a_9\bar{x}\bar{y}^2 + a_{10}\bar{x}^2\bar{y}^2 + \bar{y}/c[a_{11}(\bar{x}^2 - \bar{y}^2) + a_{12}\bar{x}^2\bar{y}^2 + a_{13}(\bar{x}^4 - \bar{y}^4)] \quad (2)$$

Δx , Δy	correction terms for formulating the camera's systematic errors
$\Delta x_p, \Delta y_p, \Delta c$	changes in PPAC and focal length
K_1, K_2 and K_3	radial lens distortion parameters
P_1 and P_2	decentring lens distortion parameters
a_1, and a_2	affinity and shearing parameters
a_3, to a_{13}	irregular distortion parameters

where

$$\bar{x} = x - x_p$$

$$\bar{y} = y - y_p$$

$$r^2 = \bar{x}^2 + \bar{y}^2$$

However, there are certain issues with the self-calibration method:

- Treatment of additional parameters as block or photo invariants or combinations of both
- Operational problems; that is, the total strategy of assessing blunders, errors in control points, and systematic errors
- The determinability checking of APs; that is, excluding indeterminable APs from the system
- Significance testing of APs

Each one of the above issues requires careful evaluation and proper use of the APs. The successful solution of the normal equations of the self-calibrating bundle adjustment is governed by the extent of the *correlation* between the unknown parameters (AP coefficients, exterior orientation (EO) parameters, and object coordinates). If any two parameters, for instance, are highly correlated, both tend to perform the same function. In such a case, one or the other can be suppressed without losing much information.

Therefore, it is very important to study the correlation structure of unknown parameters and to check the determinability of APs.

3.4 Correction Grid by Collocation Adjustment

This method does not really belong to the camera calibration methods mentioned above. In this method, some a posteriori interpolation treatment is performed on the image residuals of a bundle block adjustment. Calculated mean image residuals then serve as correction values at the interpolation points of the grid. The correction grid is able to remove the systematic errors in the image plane that could not be computed or modeled by APs in a self-calibration bundle adjustment. This correction grid application works the same way as "Reseau" to refine image coordinates for the local systematic errors by bi-linear interpolation (Madani, 2008).

4. RMK D CALIBRATION PROCEDURE

RMK D is geometrically calibrated with two methods: a laboratory calibration followed by an airborne calibration. In the laboratory calibration, the lens distortion and initial values of the focal length and principle point coordinates are estimated. Then the test field calibration computes the camera's remaining distortion and the final values of the interior orientation parameters.

In this study, two laboratory camera calibration procedures are used to estimate the lens distortion parameters:

1) Bundle Adjustment with Australis Model
2) Z/I Grid Model

The RMK D camera is mounted on two rotation tables (Figure 2) that can be rotated about two axes. The image coordinates of about 403 points on 20 lines that are distributed diagonally on the focal plane are automatically measured by finding the center of a light with a precision of about 0.1 of a pixel (Figure 3). The light point is mapped from the "infinity" using a collimator (Doerstel, et al, 2003).

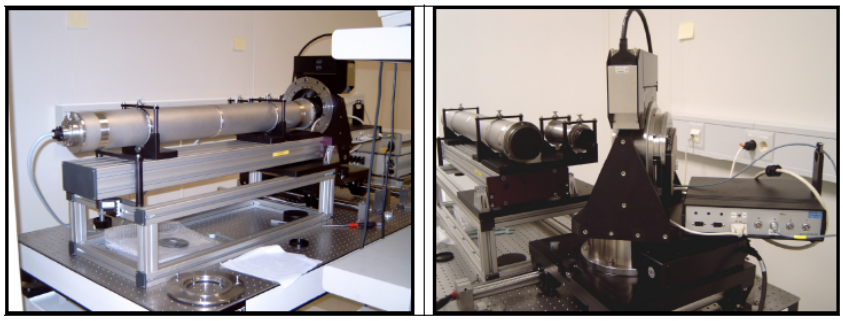

Figure 2. Lab calibration at Zeiss Jena

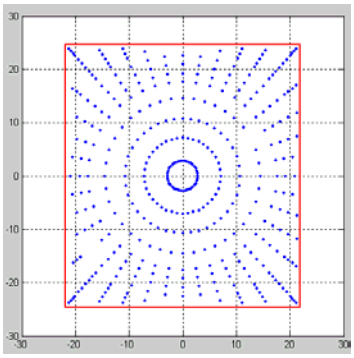

Figure 3. Collimator calibration pattern (20 lines and 403 points)

4.1 Bundle Adjustment with Australis Model

The Australis model, a sub-set of Brown model has the following form (Beyer (1992, Fraser, 1997) :

$$\Delta x = \Delta x_p - (\bar{x}/c)\Delta c + a_1\bar{x} + a_2\bar{y} + \bar{x}[K_1 r^2 + K_2 r^4 + K_3 r^6] + P_1(r^2 + 2\bar{x}^2) + 2P_2\bar{x}\bar{y}$$
$$\Delta y = \Delta y_p - (\bar{y}/c)\Delta c + \bar{y}[K_1 r^2 + K_2 r^4 + K_3 r^6] + 2P_1\bar{x}\bar{y} + P_2(r^2 + 2\bar{y}^2) \qquad (3)$$

In this self-calibrating bundle adjustment, the object points and the camera exposure stations (X_C, Y_C, Z_C) are fixed, and the image point coordinates (x, y) are weighted with the standard deviation of 0.1 of a pixel. The unknowns are the camera's rotation angles and the parameters of the Australis model.

The location of the principal point is not defined for most digital cameras and varies from camera to camera with the precision at which sensors are mounted into cameras and depends on the configuration of the frame grabber. Due to the weak block geometry (flat "test field" and vertical imagery), it is also not possible to estimate the principal point of auto collimation since these parameters are highly correlated with the exterior orientation angles ω, ϕ and the decentering distortion parameters P_1, P_2.

4.2 Z/I Grid Model Adjustment

In this method, the collimator observations are treated as direct measurements of camera distortion such that nominal dialed angular positions of the rotation stand are reduced to a focal plane of 45mm and offset to a rotation center of symmetry to become control or "fiducial" coordinates. Distortion is the difference between measured and fiducial coordinates. When the collimator beam does not move in the CCD plane under the rotation stand moving in "swing" direction "η", it is approximately aligned with the camera axis. Since the CCD is placed into the focal plane such that MTF (Modulation Transfer Function) distribution is maximized across the frame, the imaging plane has minimal tip and tilt with respect to rotational center of symmetry. Thus, tip and tilt of the camera with respect to the object plane of the collimator 20-line pattern can be neglected in calibration and later recovered via exterior orientation parameters and PPAC in photo triangulation. The remaining swing (azimuthal) offset between the collimator reference and camera reference can be estimated and subtracted from the fiducial coordinates. ZI Grid simply provides the

smoothing interpolation on a regular grid between star-pattern distortions recorded by the camera from rotating around a stationary collimator. This is done in three steps described below.

4.2.1 Calibration of Principal Point of Best Symmetry (PPBS) and CCD Common Rotation (Swing) Offset

Composite lens-CCD distortion is dominated by a radial term: ~400μm in the radial direction and ~1-3μm in the tangential direction. Thus, a principal point of best symmetry (PPBS) of the distortion presented in polar coordinates can be found by minimizing the tangential distortion with the simultaneous account for a common in-plane rotation between the collimator zero-reference in the rotational direction (object coordinate space) and the one of the CCD (camera coordinate system).

Let control point coordinates reduced to a nominal focal plane be x and y, and Cartesian image observations converted from raster space to camera space be u and v.

Then, the tangential distortion component with respect to unknown PPBS (u_{pp}, v_{pp}) is

$$v_t = -\sin(\eta)\cdot(u - u_{pp} - x) + \cos(\eta)\cdot(v - v_{pp} - y) - r\cdot\eta_0 \tag{4}$$

where $\eta = \tan^{-1}(y/x)$ and η_0 is a small common rotation angle in radians between (x, y) and (u, v) spaces.

The problem of minimizing v_t from a system of 403 condition equations (corresponding to all observations beside the ones near the CCD center) is solved for three unknown parameters u_{pp}, v_{pp}, η_0.

As an example, the calibrated PPBS and the common CCD rotation are u_{pp} = -0.010285 mm, v_{pp} = -0.028632 mm, η_0 = 0.00011972 radians (0.0069 degrees), respectively.

The refined control space is defined by

$$x' = \cos(\eta_0)x + \sin(\eta_0)y;\; y' = -\sin(\eta_0)x + \cos(\eta_0)y \tag{5}$$

The refined observation space is defined by

$$u' = u - u_{pp},\quad v' = v - v_{pp}. \tag{6}$$

4.2.2 Calibration for Radial Symmetric Distortion

Radial and tangential distortions with respect to the calibrated PPBS and reduced by a common rotation η_0 are given in Figure 4. One can clearly see that the dominant radial trend is quite centrally symmetric and the dominant trend can be captured by a radial symmetric 1-D polynomial. The result of fitting a 7th order (7 full-power parameters) polynomial (Equations 6-7) is shown in the lower plot of Figure 4.

$$v_r = \cos(\eta')\cdot(u' - x') + \sin(\eta')\cdot(v' - y'),\quad \eta' = \tan^{-1}(y'/x') \tag{7}$$

$$\hat{v}_r = p_1\cdot\bar{r} + p_2\cdot\bar{r}^2 + p_3\cdot\bar{r}^3 + p_4\cdot\bar{r}^4 + p_5\cdot\bar{r}^5 + p_6\cdot\bar{r}^6 + p_7\cdot\bar{r}^7 \tag{8}$$

$r = \sqrt{x^2 + y^2}$, $\bar{r} = r / \max(r)$.

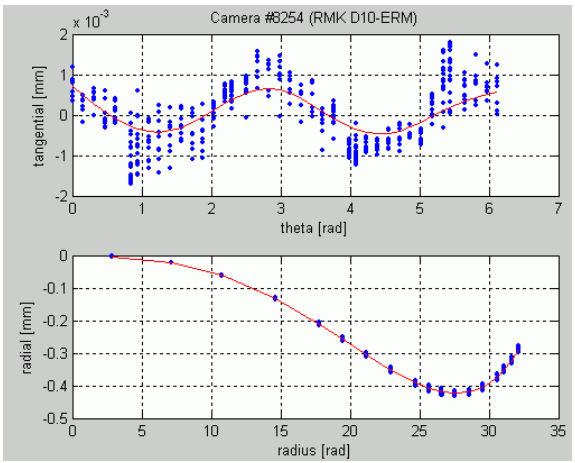

Figure 4. A 20-line collimator calibration pattern of 403 points

4.2.3 Calibration for Non-Symmetric Radial and Tangential Distortions

The remaining systematic distortions (left after subtracting the dominant radial trend with a proper centering of its best symmetry) do not exceed 10 microns but still exhibit a strong correlation shape of astigmatic and de-centering type. The de-centering does not come from the multi-lens system itself but rather from the shift in radial distortion shapes of the lens and the CCD chip (the dominant chip un-flatness is also radially symmetric resembling radial lens distortion and they are shifted with respect to each other). Also, one should not forget the influence of uncompensated camera boresight in tip/tilt directions.

Two global thin-plate splines have been fitted to the remaining non-symmetric radial and tangential distortions (see Figure 5).

One can observe in Figure 5 that the tangential observations exhibit more noise than the remainder of the radial distortions, which corresponds to the difference in angular accuracy of the collimator along two rotational axes.

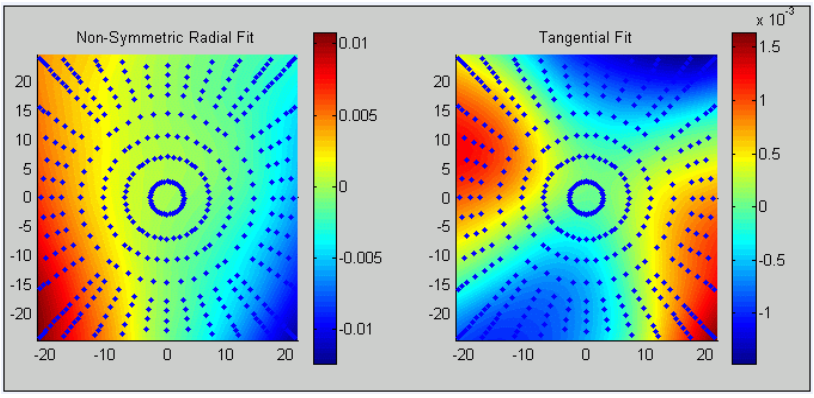

Figure 5. Fitting non-symmetric radial and tangential distortions

4.2.4 Total Distortion Shape and Grid Calibration Residuals

The shapes of final total centrally-symmetric and non-symmetric distortions, for both models, are given in Figure 6. We can conditionally call them radial and de-centering parts. Residuals for the collimator measurements shown in Figure 3 are plotted in Figure 7. As can be seen, the remaining distortion residuals are random and the maximum value is about 1 micron.

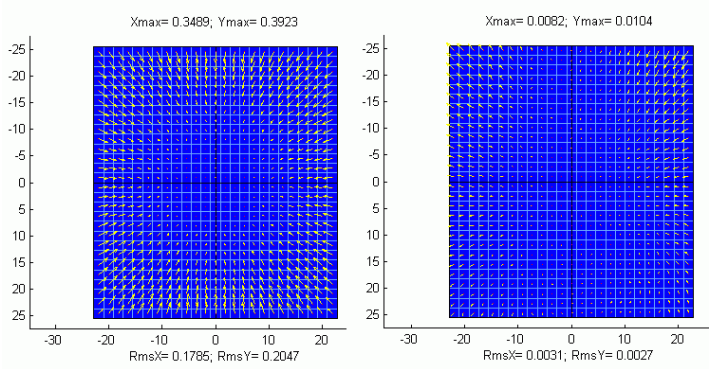

Figure 6. Final radial symmetric and non-symmetric distortion estimates

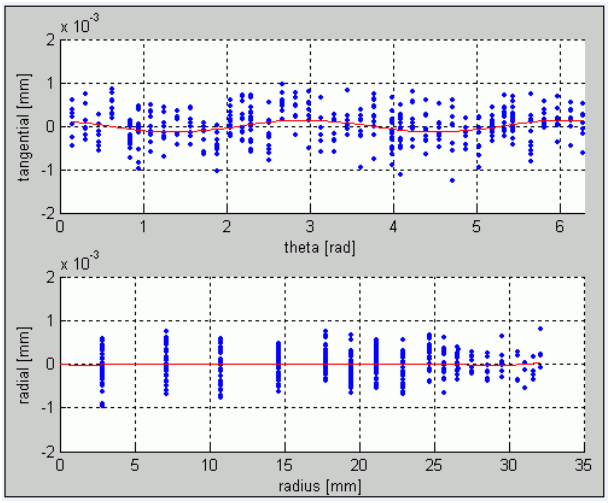

Figure 7. Remaining calibration residuals for 403 collimator measurements in mm

5. CALIBRATION QUALITY CONTROL VIA AERIAL TEST BLOCK

In order to check the quality of the lab calibration and to compute (model) the remaining systematic errors and the camera interior orientation parameters, a block of 66 images with a cross strip of 5x6 flown over a test field in Aalen, Germany, with high-quality GPS/INS and 17 control points have been used (Figure 8).

The RMK D images were postprocessed with the calibration parameters estimated by the Australis model and the Z/I Grid model. Aerial triangulations were performed on these two blocks by the ImageStation Automatic Triangulation (ISAT) product (Madani, 2001).

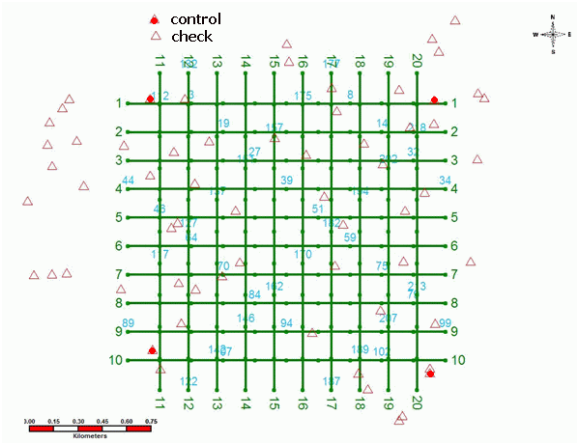

Figure 8. Distribution of control and check points

5.1 Collocation Grid Calibration

Collocation grids have been computed using all 17 control points and GPS for these two blocks. Then, the adjustment results are tested for maximal bending with only 4 control points. Figure 9 shows the collocation grids' residuals after the Australis and the Z/I grid models. Figure 10 shows that the uncompensated distortion errors by the Z/I grid model is 1/3 of the Australis model.

The test block results with/without collocation for "Australis Distortion Block" and "Z/I Grid Distortion Block" are shown in Tables 1 and 2, respectively. One can clearly see that a collocation grid makes a more uniform fit into the check points, but RMSZ bending in vertical direction did not change drastically. So, existence of a collocation grid for camera calibration is not very critical for this camera.

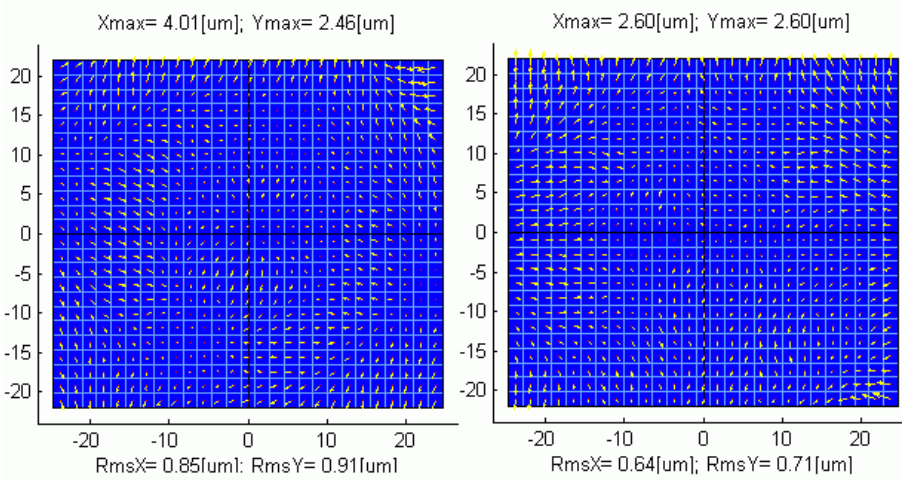

Figure 9. Collocation grids after Australis (left) and Z/I (right) Models

5.2 Self-Calibration Adjustment

Self-calibration bundle adjustments using the Ebner model were also performed on these two blocks. The bundle adjustments with and without self-calibration and the remaining

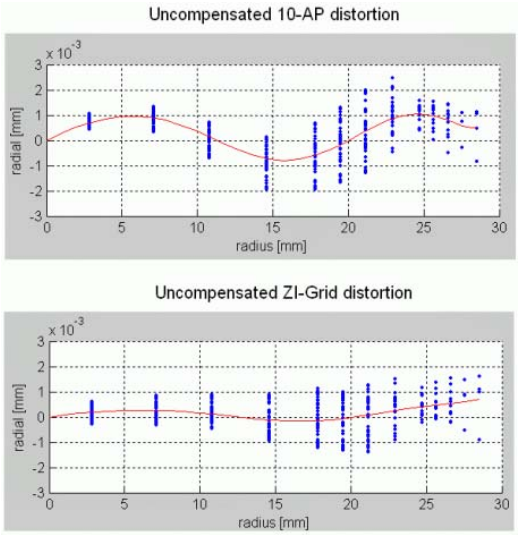

Figure 10. Collocation grid projection in radial direction

systematic errors using the significant additional parameters are shown in Table 3 and Figure 11, respectively).

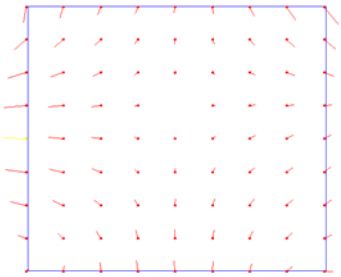

Figure 11. Self-calibration grids of the Australis and Z/I Grid Blocks

Again, self-calibration makes a more uniform fit into control points, but it is not essential for the Z/I Grid block (maximum remaining distortion is 2µm).

Table 1. AT Results of Australis Distortion Block

Block Geometry	Control Point Distribution	Australis Distortion Model					
Number of Photos (Overlaps)	Number of Control / Check	Correction Grid Off			Correction Grid On		
		RMS – Check Points (m)			RMS – Check Points (m)		
		X	Y	Z	X	Y	Z
66 (60 / 60 %)	4 /14	0.046	0.031	0.101	0.033	0.032	0.074
	5 / 13	0.046	0.032	0.101	0.033	0.033	0.076
18 (60 / 30 %)	5 / 6	0.042	0.032	0.156	0.032	0.040	0.129
	4 / 7	0.037	0.030	0.179	0.033	0.037	0.124

Table 2. AT Results of Z/I Grid Distortion Block

Block Geometry	Control Point Distribution	Z/I Grid Distortion Model					
Number of Photos (Overlaps)	Number of Control / Check	Correction Grid Off			Correction Grid On		
		RMS – Check Points (m)			RMS – Check Points (m)		
		X	Y	Z	X	Y	Z
66 (60 / 60 %)	4 /14	0.042	0.027	0.072	0.038	0.032	0.065
	5 / 13	0.044	0.027	0.074	0.040	0.032	0.066
18 (60 / 30 %)	5 / 7	0.039	0.038	0.039	0.023	0.034	0.040
	4 / 8	0.035	0.032	0.056	0.022	0.031	0.050

Table 3. AT Results of Australis and Z/I Grid Blocks

Block	14 Control	Self-Calibration Off			Self-Calibration On		
Australis Distortion	RMS (m)	0.021	0.027	0.022	0.018	0.021	0.019
	Max (m)	0.044	-0.047	-0.037	0.045	-0.042	-0.033
Z/I Grid Distortion	RMS (m)	0.017	0.017	0.012	0.015	0.018	0.014
	Max (m)	0.029	0.038	0.052	-0.027	0.041	0.055

6. CONCLUSIONS

Section 4 of this paper has presented a direct method of camera calibration for systematic lens-CCD distortions. It is shown that the "Z/I Grid" method provides adequate calibration such that post-correction via self-calibration or collocation using aerial data is not critical.

Maximal uncompensated distortion is around 2µm and it does not cause severe bending of the block DTM; i.e. its propagation to object space is limited. At 8cm GSD, this camera achieves an accuracy of about ½ GSD in XY and 0.6 GSD in Z for the worst block configuration (only 4 corner controls and no cross-strips).

7. REFERENCES

Beyer, H. (1992): Geometric and Radiometric Analysis of a CCD-Camera Based Photogrammetric Close-Range System, Institut für Geodäsie und Photogrammetrie, an der Eidgenössische Technische Hochschule, Zürich, Dissertation ETH Nr. 9701.

Brown, D. (1976): The bundle adjustment - progress and prospects, IAP, Vol. XXI, Part 3, Commission III, pp. 1-33, ISP Congress Helsinki.

Doering D., Hildebrand J., Diete N. (2009): Advantages of customized optical design for aerial survey cameras, Photogrammetric Week 2009, Stuttgart, Germany.

Dörstel C., (2009): RMK D - A True Metric Medium-Format Digital Aerial Camera System practical experience and accuracy assessment, Photogrammetric Week 2009, Stuttgart, Germany.

Fraser, C. (1997): Digital camera self-calibration, JPRS, April, Vol. 52, No. 4, pp. 149-159.

Madani, M., Shkolnikov, I. (2008b): Increasing Geometric Accuracy of DMC's Virtual Images, ISPRS Congress 2008, Beijing, China.

Madani, M., Shkolnikov, I. (2008a): International Calibration and Orientation Workshop, January 30th – February 1st, 2008, Castelldefels, Spain.

Madani, M (2001): Z/I Imaging New Automatic Aerial Triangulation System, ASPRS Annual Conference, St. Louis, MO, April 23-27, 2001.

Madani M., (1985): Accuracy Potential of Non-Metric Cameras in Close-Range Photogrammetry Ph.D. Dissertation, Department of Geodetic Science and Surveying, The Ohio State University.

Ryan R., Pagnutti M. (2009): Enhanced Absolute and Relative Radiometric Calibration for Digital Aerial Cameras, Photogrammetric Week 2009, Stuttgart, Germany.